Journal of
Marine Science and Engineering

MDPI

Article

A Multi-Objective Optimization of the Anchor-Last Deployment of the Marine Submersible Buoy System Based on the Particle Swarm Optimization Algorithm

Xiaohan Chen, Bing Liu and Guigao Le *

School of Mechanical Engineering, Nanjing University of Science and Technology, Nanjing 210094, China
* Correspondence: leguigao@njust.edu.cn

Abstract: Marine submersible buoy systems hold significant value as critical equipment in marine science research. This study examines a marine submersible buoy system that includes an anchor block, mooring line, battery compartment, power supply cable, and submersible buoy. The anchor-last deployment method is a conventional strategy for deploying marine submersible systems. Initially, the other components are positioned on the sea surface, followed by the deployment of the anchor block from the ship's deck. The anchor block will pull the battery compartment and submersible buoy into the water and eventually sink to the seabed. In this deployment process, ocean currents have a relatively large impact on the anchor block's landing position. Increasing the weight of the anchor block will make the anchor block land on the seabed sooner, which can minimize the impact of ocean currents. However, an overabundance of weight can generate a significant strain on both the cables, potentially resulting in cable breakage. In order to find the parameters that can make the anchor block reach the seabed as soon as possible and ensure that the tension force of the cables does not exceed the maximum, a dynamic model of the deployment process is established based on computational fluid dynamics (CFD) and solved using the Runge–Kutta method of the fourth order. Particle swarm optimization is employed to optimize the key parameters. The penalty function is used to constrain the particle space. The findings indicate that the utilization of particle swarm optimization is efficacious for optimizing the parameters of submersible buoy systems for marine applications. Optimized parameters allow the anchor block to reach the seafloor quickly and the tension on the cables to not exceed the given value.

Keywords: submersible buoy system; anchor-last deployment; multi-objective optimization; particle swarm optimization

check for updates

Citation: Chen, X.; Liu, B.; Le, G. A Multi-Objective Optimization of the Anchor-Last Deployment of the Marine Submersible Buoy System Based on the Particle Swarm Optimization Algorithm. *J. Mar. Sci. Eng.* **2023**, *11*, 1305. https://doi.org/10.3390/jmse11071305

Academic Editor: Sergei Chernyi

Received: 14 May 2023
Revised: 19 June 2023
Accepted: 21 June 2023
Published: 27 June 2023

Copyright: © 2023 by the authors. Licensee MDPI, Basel, Switzerland. This article is an open access article distributed under the terms and conditions of the Creative Commons Attribution (CC BY) license (https://creativecommons.org/licenses/by/4.0/).

1. Introduction

The need for underwater monitoring technology is growing rapidly as underwater research becomes more in-depth. Coastal defense, underwater communication, and underwater environment research are all common uses for submersible buoys. Because they are practical, recyclable, and effective, they have several applications in the fields of information collection and underwater environmental monitoring. They have been widely used in ambient sea-noise acquisition [1–3], marine fouling monitoring [4], and marine seismic surveillance [5].

In this paper, a submersible buoy system consisting of an anchor block, battery compartment, and submersible buoy is studied. These components are connected by cables, as shown in Figure 1.

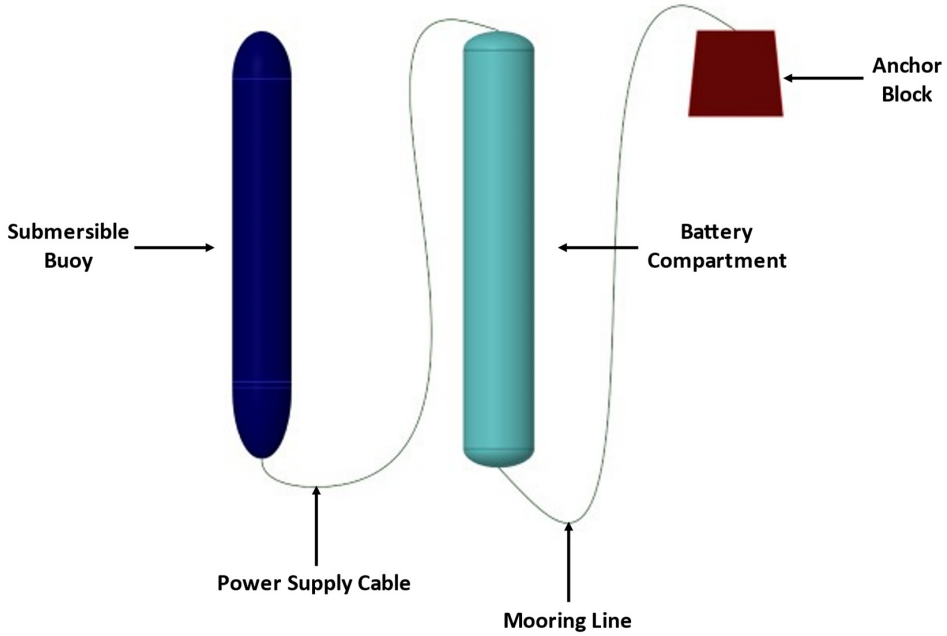


Figure 1. Components of the marine submersible buoy system and their interconnection.

Before using a submersible buoy system, it must be deployed in a specific sea area where underwater monitoring is required. Anchor-last deployment is a widely used approach to deploying an underwater mooring system. At first, the submersible buoy and battery compartment are placed on the sea surface. The anchor block is deployed at the end. Due to the heavy weight of the anchor block, it will drop quickly after being deployed into the water and pull the other component to sink with it. Eventually, it will drag the entire system down to the seabed. As shown in Figure 2, due to gravity and the large downward velocity of the anchor block, a large tension will be successively generated on the cables when pulling the system into water. The deployment will fail if the cables are broken by large tension forces. To study the dynamic mechanical behavior of the system during deployment, this paper establishes dynamic equations for the anchor-last deployment.

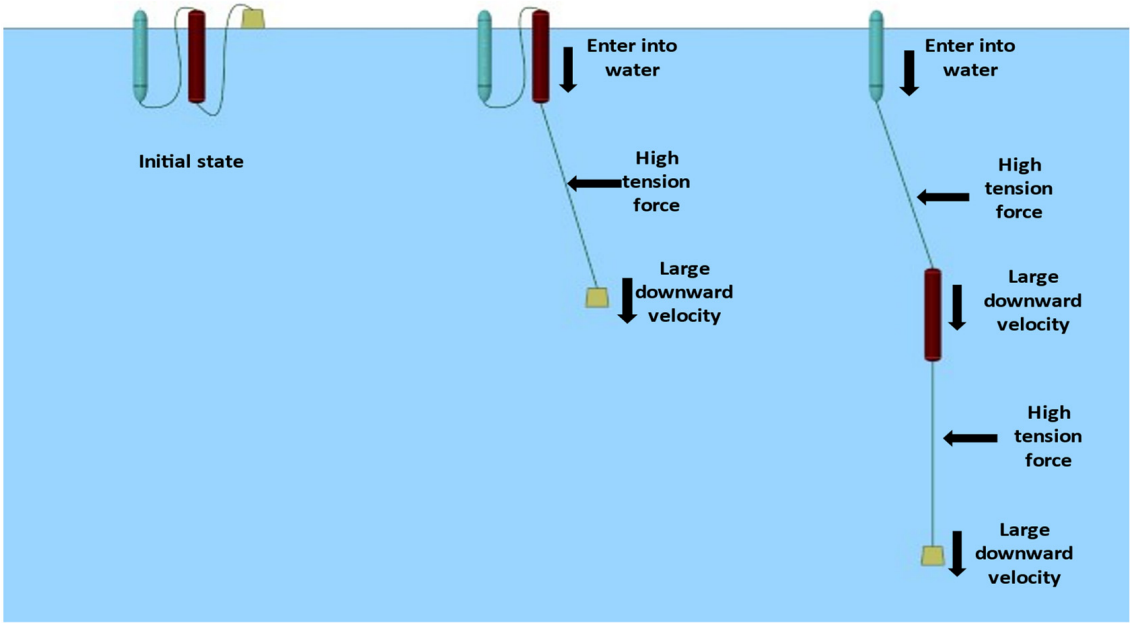


Figure 2. The deployment process of a marine submersible buoy system.

The landing position of the anchor block is essential for efficient use. Figure 3 illustrates that ocean currents have a relatively large impact on the landing position. Obviously, increasing the weight of the anchor block will make it reach the seabed sooner and reduce the impact of ocean currents. However, an increased mass of the anchor block will result in a higher tensile load on the cables.

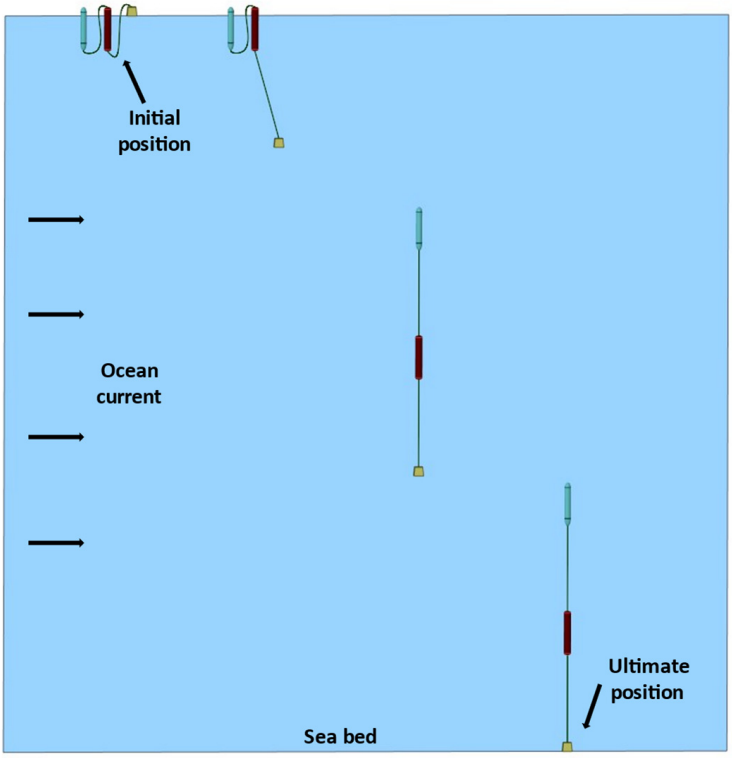


Figure 3. Ocean currents impact on the ultimate landing position.

Increasing the cable length can reduce the cable tension. However, an excessive length will cause the submersible buoy to deviate from a certain water level, which will reduce the efficiency of the marine environmental exploration. The sum of the lengths of the two cables should not exceed a given value. In addition, the stiffness and maximum bearing capacity of the mooring line and power supply cable are different. How to distribute the lengths of these two types of cables to ensure that their tension does not exceed the maximum bearing capacity under given circumstances is a problem.

In this paper, a dynamic model of the deployment process is established to study the dynamic mechanical behavior of these cables. Particle swarm optimization is an intelligent optimization algorithm that was proposed by Kennedy and Eberhart [6]. The particle swarm optimization algorithm is inspired by the results of the modeling and simulation of bird colony behavior. With the rapid progress of computer performance, particle swarm optimization has been widely applied to linear optimization problems, nonlinear optimization problems, and multi-objective optimization problems. In this paper, particle swarm optimization is adopted to optimize the key parameters of a submersible buoy system. First, CFD is applied to calculate the hydraulic resistance and inertia resistance of the components in the submersible buoy system. The numerical method is validated by comparing the hydraulic resistance with the experimental results. Then, the dynamic equations of the deployment process are established. The dynamic mechanical behavior of marine submersible buoy systems can be obtained by solving the dynamic equations using the Runge–Kutta method of the fourth order. At last, the submersible buoy system is optimized using the particle swarm optimization algorithm to determine its key parameters.

2. Background

In recent years, marine submersible buoy systems and underwater mooring systems have been studied by many scholars. N. A. Shul'ga and A. I. Bezverkhii (2004) presented a methodology for obtaining the equations of motion for one-dimensional discrete-continuous flexible systems with one-sided deformation characteristics [7]. Wang Jing and Luan Xiwu (2010) employed the finite element numerical simulation method in conjunction with abaqus software to determine the optimal material strength for submarine buoy shells and assess their deformation characteristics under external pressure [8]. The ultimate goal of their investigation was to develop a suitable shell design. Binbin Lai et al. (2014) conducted a study on a representative sea condition found in the coastal regions of China [9]. The study focused on the development of a new semi-submersible foundation for offshore wind turbines that could be utilized in water depths of up to 200 m. Dongsheng Qiao et al. (2014) conducted a numerical simulation in the time domain to examine the impact of buoy systems on the dynamics of mooring systems and motion responses of a semi-submersible platform [10]. The study aimed to investigate the global responses of the platform. Zhanfeng Qi et al. (2014) developed a dynamic model of the submersible buoy system using the lumped mass method, followed by a subsequent dynamic analysis [11]. Tsukada et al. (2014) introduced a semi-empirical framework that employed hydrodynamic coefficients obtained for cylinders with low aspect ratios [12]. To ensure the precision of their numerical simulations, the outcomes were cross-referenced with experimental data that had been documented in scholarly sources, revealing a favorable level of conformity. Diener V. R. Fontoura et al. (2015) employed the VIM calibrated wake oscillator model to replicate certain reduced model tests of Free-standing hybrid risers for the purpose of validating the precision [13]. The study compared its experimental results with the numerical simulation results for the amplitude and frequency of the oscillation against the reduced velocity. Chunyan Ji and Zhiming Yuan (2015) introduced a novel hybrid mooring system [14]. To optimize the motion performance of the platform and alleviate the vertical forces exerted on the lower end of the mooring lines, a series of weights and buoys were deliberately placed at strategic intervals along each segment of the mooring lines. The deployment dynamics of submersible buoy systems were investigated by Zheng Zhongqiang et al. (2016) through the use of both numerical and experimental approaches [15]. Upon comparing the outcomes of the two approaches, it was determined that the numerical model effectively replicated the factual procedure and circumstances of the experiment. The simulation outcomes exhibited a high degree of concurrence with the experimental findings, encompassing the gravity anchor's placement and the velocities of the distinct nodes of the submersible buoy. Jiahao Chen et al. (2018) conducted model testing investigations on a spar-buoy and semi-submersible floating wind turbines and performed comparative analyses on the experimental outcomes of the two types of floating wind turbines [16]. Hamidreza Ghafari et al. (2018) conducted an analysis of the frequency and time responses of a semi-submersible platform subjected to a combination of wind and wave loads [17]. Jun Yan et al. (2018) introduced an optimized mooring system that utilized submerged buoys and was based on a conventional catenary mooring system [18]. Simulations of hydrodynamics and acoustics were carried out by Qun Yang et al. (2019) in order to evaluate the effect that vertical cable orientations have on the performance of undersea systems while they are being tested [19]. The study involved comparing the hydrodynamic coefficients and rear velocity distribution of various vertical cable forms, as well as evaluating the subsurface submerged standard flow noise of different vertical cables. The aim was to identify the optimal vertical cable format. Yue Zhang et al. (2019) conducted a numerical simulation study to evaluate the flow noise of a submersible buoy in a rational manner [20]. The numerical model employed the large eddy simulation technique in conjunction with the finite element method and automatically matched layer method. Zhilei Zhang et al. (2019) presented a real-time data acquisition system that was specifically developed for a submersible buoy [21]. The system was designed to address the requirements of low power consumption and high-speed data transmission. Imanol Touzon et al. (2020) proposed an

approach for modelling the interaction among supporting structures and mooring systems that is introduced through kinematic relations. The proposed approach was validated with the experimental wave tank [22]. Srinivasan Chandrasekaran et al. (2021) undertook a research investigation concerning coupled dynamic analyses of a semi-submersible platform located in the deep waters of the South China Sea region. [23]. The study examined the platform's response to the potential damage of the restraining system for both 10- and 100-year return period events. The study conducted by Xueping Rong et al. (2021) focused on the semi-submersible floating foundation design of offshore wind turbines [24]. Specifically, the research delved into the mooring system of semi-submersible floating foundations, which was designed based on its structural parameters. The design involved the use of four buoys. Chiemela Victor Amaechi et al. (2022) provided a comprehensive analysis of the motion characterization of the Catenary Anchor Leg Moorings (CALM) buoy hose system. The CALM buoy is a buoyant structure that exhibits six degrees of freedom [25]. They presented a comprehensive experimental analysis of the CALM buoy hose model, which was conducted in the Wave Tank at Lancaster University. The study employed three innovative techniques to provide a detailed and thorough presentation of its results. Then (2022), numerical investigations were conducted to examine the performance of the CALM buoy [26]. Xiaohan Chen et al. (2022) conducted a research investigation on the deployment of submersible buoys utilizing the VOF method and lumped mass method [27]. Dongdong Han et al. (2022) applied a method for designing a tuned mass damper as a passive structural control strategy for semi-submersible floating offshore wind turbines [28]. The aim was to reduce the response of the turbines to combined winds and waves. Menghao Li and colleagues (2022) proposed an underwater acoustic geodetic network configuration consisting of three seafloor base stations, one subsurface buoy, and one sea surface buoy, with the aim of offering high-precision kinematic positioning for underwater submersibles [29]. Atefeh Neisi et al. (2022) presented two hybrid mooring systems aimed at enhancing the dynamic motion performance of floating platforms [30].

It can be seen from the completed research that direct CFD simulation on a submersible buoy system is feasible [27]. However, when the submersible buoy system is deployed in a sea area that is hundreds of meters deep, the computational area is too large. The computation process would be very time consuming. Multi-body dynamics are an effective and simple way of simulating the deployment process of a marine submersible buoy system. Comparisons between the results of multi-body dynamics and experimental results have been carried out in previous studies [15]. These results show good agreement. On the foundation of previous research, dynamic equations based on multi-body dynamics are established in this paper. In order to obtain the motion feature of the components and the tension on the cable, the dynamic equations are solved using Runge–Kutta method of the fourth order. Based on the dynamic model, the particle swarm optimization algorithm is applied to optimize the key parameters.

3. Hydraulic Resistance Calculation

3.1. Numerical Method

The CFD model uses the Navier–Stokes equations of incompressible fluid and the k-ε turbulence model [31]. The governing equations of incompressible fluids are solved using the finite volume method.

The three-dimensional incompressible Navier–Stokes equations in the cartesian coordinate system are established as follows:

$$\begin{aligned}
\rho\left(\frac{\partial u}{\partial t}+u\frac{\partial u}{\partial x}+v\frac{\partial u}{\partial y}+w\frac{\partial u}{\partial z}\right)&=\rho f_x-\frac{\partial p}{\partial x}+\mu\left(\frac{\partial^2 u}{\partial x^2}+\frac{\partial^2 u}{\partial y^2}+\frac{\partial^2 u}{\partial z^2}\right)\\
\rho\left(\frac{\partial v}{\partial t}+u\frac{\partial v}{\partial x}+v\frac{\partial v}{\partial y}+w\frac{\partial v}{\partial z}\right)&=\rho f_y-\frac{\partial p}{\partial y}+\mu\left(\frac{\partial^2 v}{\partial x^2}+\frac{\partial^2 v}{\partial y^2}+\frac{\partial^2 v}{\partial z^2}\right)\\
\rho\left(\frac{\partial w}{\partial t}+u\frac{\partial w}{\partial x}+v\frac{\partial w}{\partial y}+w\frac{\partial w}{\partial z}\right)&=\rho f_z-\frac{\partial p}{\partial z}+\mu\left(\frac{\partial^2 w}{\partial x^2}+\frac{\partial^2 w}{\partial y^2}+\frac{\partial^2 w}{\partial z^2}\right)
\end{aligned} \tag{1}$$

where ρ is the fluid density, t is the time, u, v, and w are the fluid velocities above the x, y, and z directions, respectively, p is the pressure, u is the fluid viscosity, and f_x, f_y, and f_z are the external forces per unit volume of fluid above the x, y, and z directions, respectively.

The turbulence mode is the k-ε turbulence model, which is a widely used model for determining turbulent eddy viscosity, energy dissipation rate, and kinetic energy. It has been shown to provide reasonable approximations for many types of flows.

The k-ε turbulence model determines the turbulent viscosity coefficient and subsequently calculates the turbulent stresses by solving two additional equations: the k-equation, representing the turbulent kinetic energy, and the ε-equation, representing the turbulent dissipation. The constraint equations of the turbulent kinetic energy k and turbulent dissipation rate ε are as follows:

$$\frac{\partial(\rho k)}{\partial t} + \frac{\partial\left(\rho k u_j\right)}{\partial x_j} = \frac{\partial}{\partial x_j}\left[\left(\mu + \frac{\mu_t}{\sigma_k}\right)\frac{\partial k}{\partial x_j}\right] + \rho(P_k - \varepsilon) \tag{2}$$

$$\frac{\partial(\rho \varepsilon)}{\partial t} + \frac{\partial\left(\rho \varepsilon u_j\right)}{\partial x_j} = \frac{\partial}{\partial x_j}\left[\left(\mu + \frac{\mu_t}{\sigma_\varepsilon}\right)\frac{\partial \varepsilon}{\partial x_j}\right] + \rho\frac{\varepsilon}{k}(C_1 P_k - C_2\varepsilon) \tag{3}$$

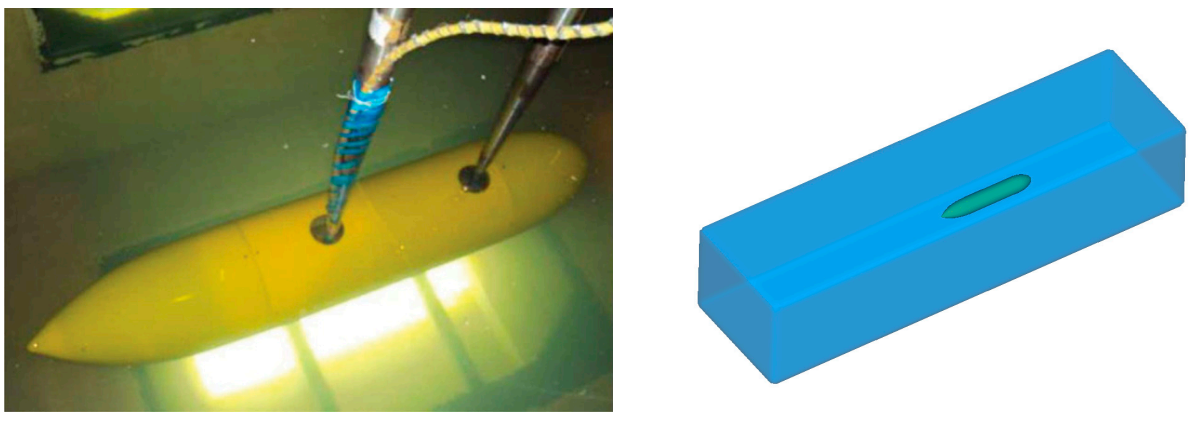
P_k is the generation term of the turbulent kinetic energy. It is defined as:

$$P_k = \frac{\mu_t}{\rho}\left(\frac{\partial u_i}{\partial x_j} + \frac{\partial u_j}{\partial x_i}\right)\frac{\partial u_i}{\partial x_j} \tag{4}$$

where u_i and u_j are the mean relative velocity components, x_i and x_j are coordinate components, μ_t is the eddy viscosity coefficient of the turbulence, and μ is the coefficient of the molecular viscosity. The constant number in the equations is defined as $C_1 = 1.44$, $C_2 = 1.92$, $\sigma_k = 1.0$, and $\sigma_\varepsilon = 1.3$.

3.2. Numerical Method Verification

In order to verify the numerical method, the water resistance of an autonomous underwater vehicle is calculated and compared to the experimental result carried out by Ting Gao et al. [32]. The experimental model and CFD model are illustrated in Figure 4.



(**a**) (**b**)

Figure 4. Experimental model and CFD model. (**a**) Experimental model of Ting Gao et al. [32]; (**b**) CFD model.

Figure 5 illustrates the boundary condition of the CFD model for the autonomous underwater vehicle. The outflow boundary condition allows fluid to flow out freely. The symmetry boundary condition applies a zero-gradient condition at the boundary, as well as a zero velocity condition normal to the boundary. The specified velocity boundary condition specifies the velocity at the boundary.

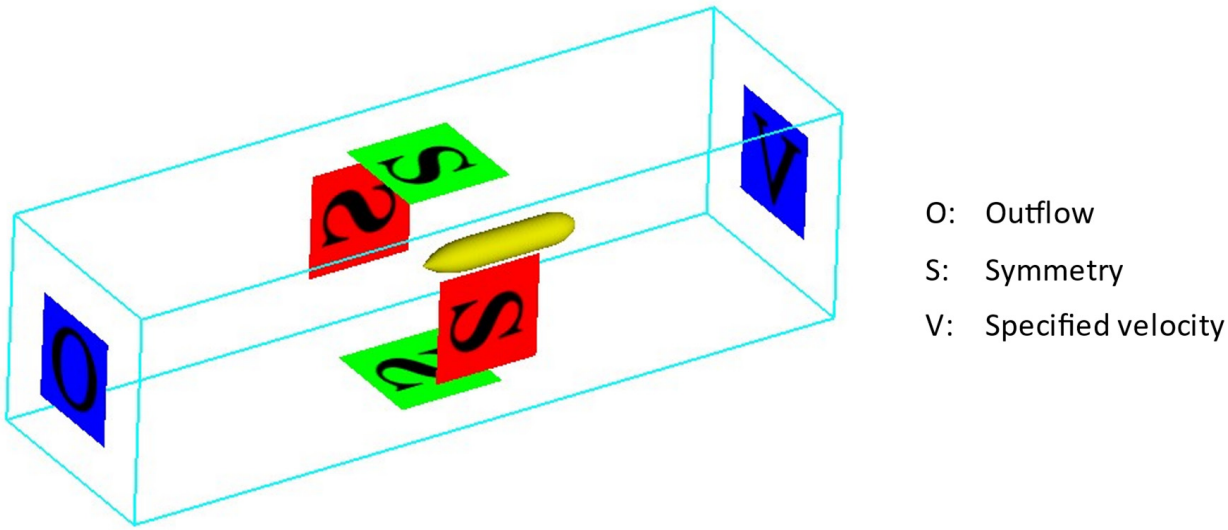


Figure 5. Boundary condition of CFD model.

The hydraulic resistance comparison of the hydraulic resistance between the experimental and CFD models is illustrated in Figure 6. The result shows a good agreement. The accuracy of the CFD model for calculating the hydraulic resistance is acceptable.

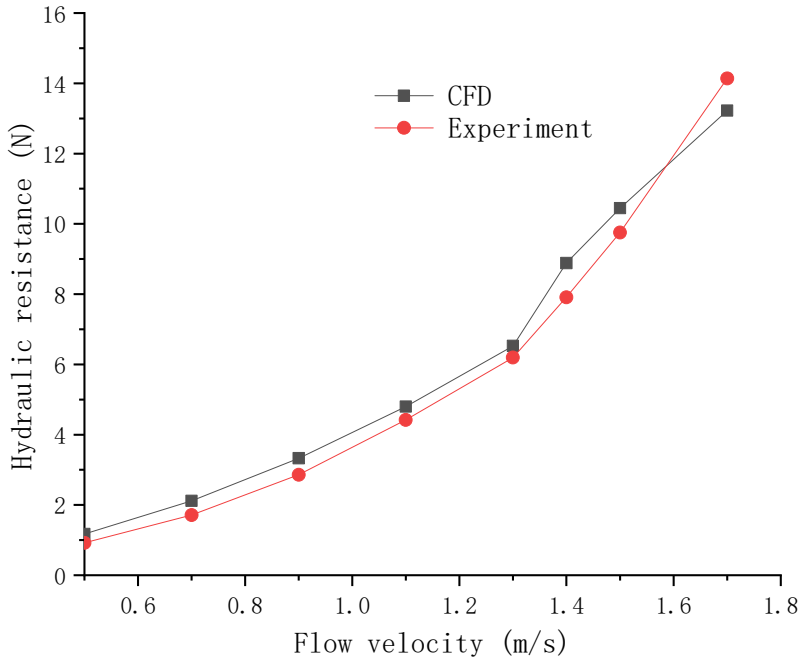


Figure 6. Comparison of hydraulic resistance between CFD result and experiment result.

3.3. Hydraulic Resistance of Components in Submersible Buoy System

The hydraulic resistance of the submersible buoy and battery compartment at several flow velocities is calculated using the CFD. Then, the hydraulic resistance is fitted using quadratic functions with a constant term of 0. Figures 7 and 8 illustrate the CFD result and fitted curves of the hydraulic resistance of the submersible buoy and battery compartment. It can be seen from Figures 7 and 8 that quadratic functions can fit well the single CFD results.

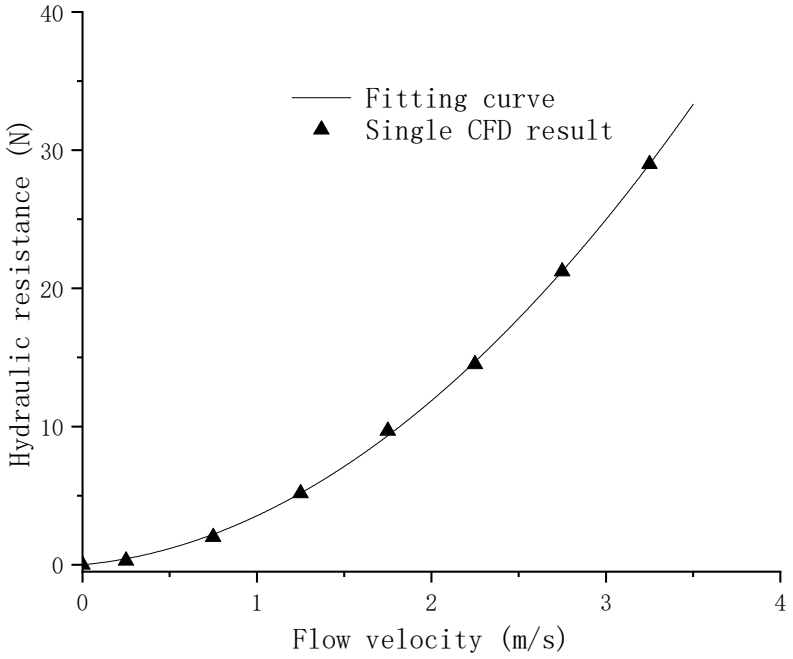


Figure 7. Hydraulic resistance of submersible buoy.

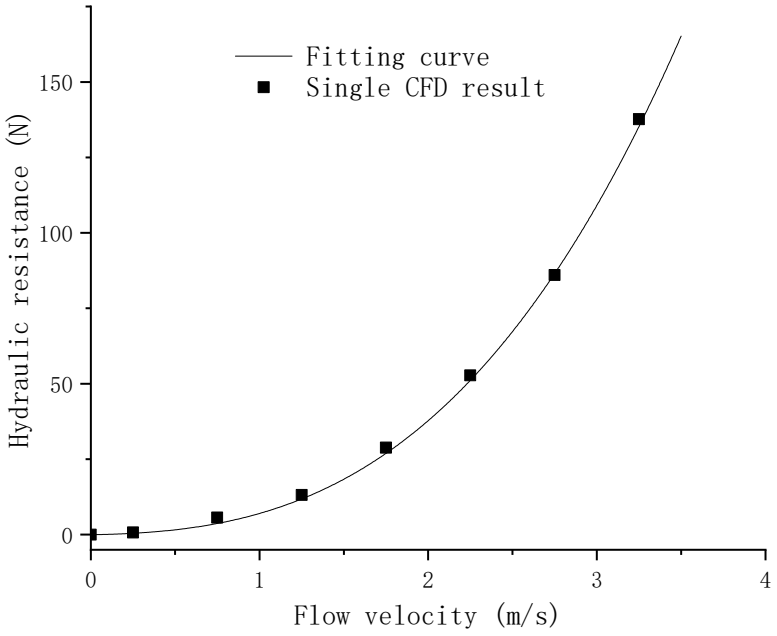


Figure 8. Hydraulic resistance of battery compartment.

The hydraulic resistance of the submersible buoy is fitted using a quadratic like,

$$D_1 = \left|2.389v_1^2 + 1.157v_1\right| \tag{5}$$

where D_1 is the hydraulic resistance of the submersible buoy and v_1 is the velocity of the submersible buoy.

The hydraulic resistance of the battery compartment is fitted using a quadratic like,

$$D_2 = \left|2.807v_2^3 + 3.443v_2^2 + 0.7605v_2\right| \tag{6}$$

where D_2 is the hydraulic resistance of the battery compartment and v_2 is the velocity of the battery compartment.

The net underwater weight of the anchor block is a parameter that needs to be optimized. The relationship between the flow velocity, net underwater weight, and flow velocity needs to be built. The different weight of the anchor block is designed in the same shape as a similar prism; therefore, the hydraulic resistance of anchor blocks under different weights is regular. The hydraulic resistance of anchor blocks under 60 kg, 80 kg, 100 kg, and 120 kg underwater net weights is calculated. The velocity varies from 0 m/s to 3.5 m/s, with the interval being 0.5 m/s. The fitting surface and single CFD results are illustrated in Figure 9.

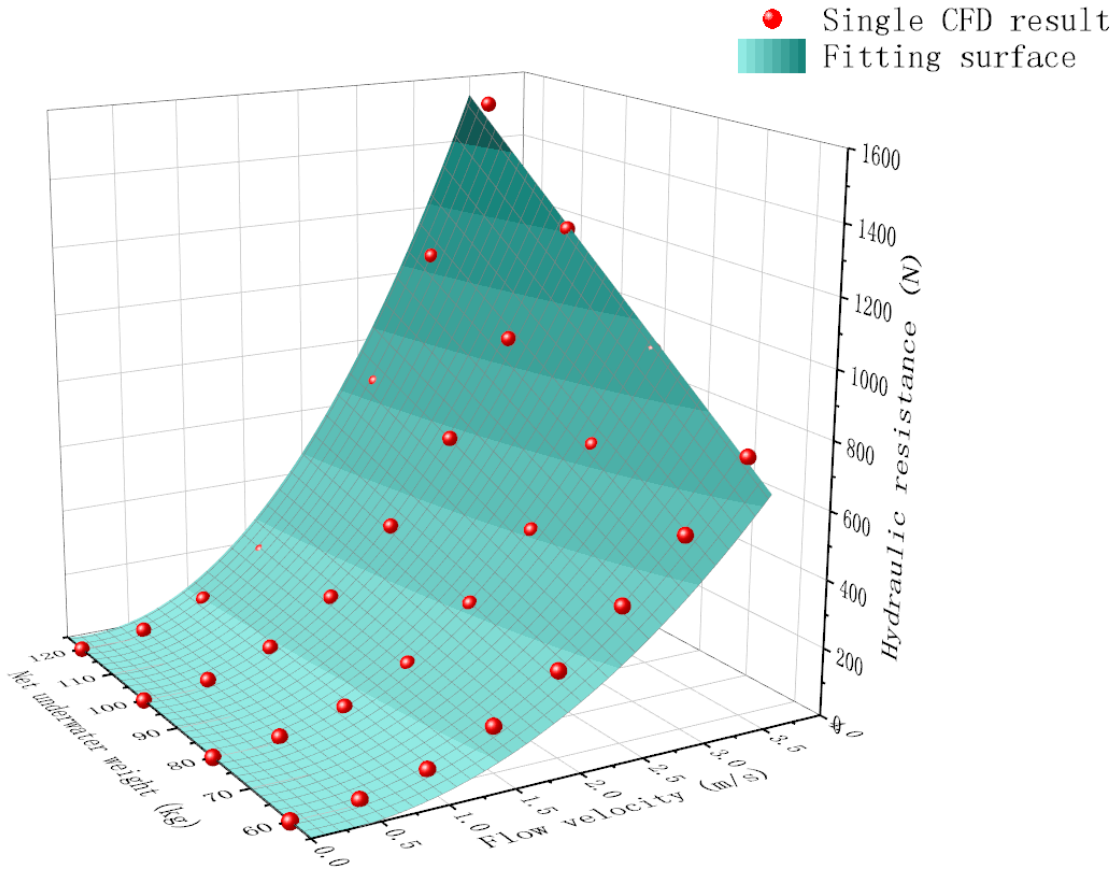


Figure 9. Hydraulic resistance of anchor block.

The hydraulic resistance of an anchor block is fitted using an equation like

$$D_3(v_3, m_3) = \left|2.465 m_3^{1.078}\left(0.3026 v_3^2 - 0.007531 v_3\right)\right| \quad (7)$$

where D_3 is the hydraulic resistance of the anchor block, m_3 is the underwater net mass of the anchor block, and v_3 is the velocity of the anchor block.

4. Dynamic Model of the Marine Submersible Buoy System

4.1. Dynamic Equations of Anchor Last Deployment Process

The deformations of the submersible buoy, battery compartment, and anchor block are far less than those of the mooring line and power supply cable. Therefore, the deformations of the submersible buoy, battery compartment, and anchor block are ignored and considered as mass points in the dynamic model. The added mass is a non-negligible parameter when studying the motion of an object in hydrodynamics. An object moves in fluid at a variable speed and the force pushing the object not only works to increase the acceleration of the object, but also to increase the acceleration of the surrounding fluid. Therefore, for an object with a certain mass to gain acceleration, the force applied to it must be greater than the product of the mass of the object and its acceleration, and this added mass is the added

mass. The added mass is related to the shape and direction of the motion of the object itself. The added mass of each component should be considered in the dynamic equations of a marine submersible buoy system. These dynamic equations are established as follows:

$$\begin{cases} \frac{d^2x_1}{dt^2}\left(m_1 + m_1'\right) = G_1 - B_1 + T_1 - D_1\left(\frac{|v_1|}{v_1}\right) \\ \frac{d^2x_2}{dt^2}\left(m_2 + m_2'\right) = G_2 - B_2 - T_1 + T_2 - D_2\left(\frac{|v_2|}{v_2}\right) \\ \frac{d^2x_3}{dt^2}\left(m_3 + m_3'\right) = G_3 - B_3 - T_2 - D_3\left(\frac{|v_3|}{v_3}\right) \end{cases} \tag{8}$$

where x_1, x_2, and x_3 are the falling distances of the submersible buoy, battery compartment, and anchor block, respectively. m_1, m_2, and m_3 are the masses of the submersible buoy, battery compartment, and anchor block, respectively. m_1', m_2', and m_3' are the added masses that are conducted by the inertia of the fluid. G_1, G_2 and G_3 are the gravity of the submersible buoy, battery compartment, and anchor block, respectively. B_1, B_2 and B_3 are the buoyancy of the submersible buoy, battery compartment, and anchor block, respectively. D_1, D_2, and D_3 are the hydraulic resistance of the submersible buoy, battery compartment, and anchor block, respectively. T_1 is the tension of the power supply cable. T_2 is the tension of the mooring line. T_1 and T_2 are calculated using the following equations:

$$\begin{cases} T_1 = \frac{E_1A_1}{l_1}\left(x_2 - x_1\right), x_2 - x_1 > l_1 \\ T_1 = 0, x_2 - x_1 < l_1 \end{cases} \tag{9}$$

$$\begin{cases} T_2 = \frac{E_2A_2}{l_2}\left(x_3 - x_2\right), x_3 - x_2 > l_2 \\ T_2 = 0, x_3 - x_2 < l_2 \end{cases} \tag{10}$$

where E_1 and E_2 are the elasticity moduli of the power supply cable and mooring line, respectively. A_1 and A_2 are the cross-sectional areas of power supply cable and mooring line, respectively. l_1 and l_2 are the lengths of the power supply cable and mooring line, respectively.

4.2. Velocity Variation of Marine Submersible Buoy

In order to obtain the velocity variation in each component in the submersible buoy system and the tension variation in each cable, the dynamic equations are solved using the Runge–Kutta method of the fourth order. This dynamic model is applied to calculate a submersible buoy system deployed in a sea area with a depth of 100 m. The anchor block is thrown into the water from a 3 m high deck with an initial velocity of 7.67 m/s. The cable lengths are 20 m for the length of the mooring line and 20 m for the length of the power supply cable. The net underwater weights of the anchor block are 150 kg, 200 kg, and 250 kg, respectively. The added mass coefficient of an object is determined by the shape of the object. Since the anchor blocks under different weights are designed to be the same shape as a similar prism, they have the same added mass coefficient of 0.6647. The parameters of the submersible buoy and battery compartment are listed in Table 1. The parameters of the mooring line and power supply cable are listed in Table 2.

Table 1. Parameters of components in submersible buoy systems.

Component	Added Mass Coefficient	Gravity	Net Buoyancy
Submersible buoy	0.0991	65 kg	152.88 N
Battery compartment	0.1086	100 kg	257.74 N

Table 2. Parameters of cables in submersible buoy systems.

Cable	Length	Elasticity Modulus	Cross Section Area
Mooring line	20 m	1273.2 MPa	19.6 mm^2
Power supply cable	20 m	636.6 MPa	78.5 mm^2

The velocity variations in the anchor block, battery compartment, and submersible buoy are illustrated in Figures 10–12. It can be seen from the results that the anchor block velocity rapidly decreases to a stable value after being thrown into the water, and then pulls the battery compartment into the water. The velocity of the battery compartment increases rapidly when it is pulled into the water. Then, the velocities of the anchor block and battery compartment exhibit a tendency of oscillation and gradual convergence. Subsequently, the submersible buoy is pulled into the water. Its velocity increases rapidly. Then, the velocities of the anchor block, battery compartment, and submersible buoy exhibit a tendency of oscillation and gradual convergence. After the anchor block sinks to the seabed, the velocities of the submersible buoy and battery compartment show a trend of oscillation and decrease.

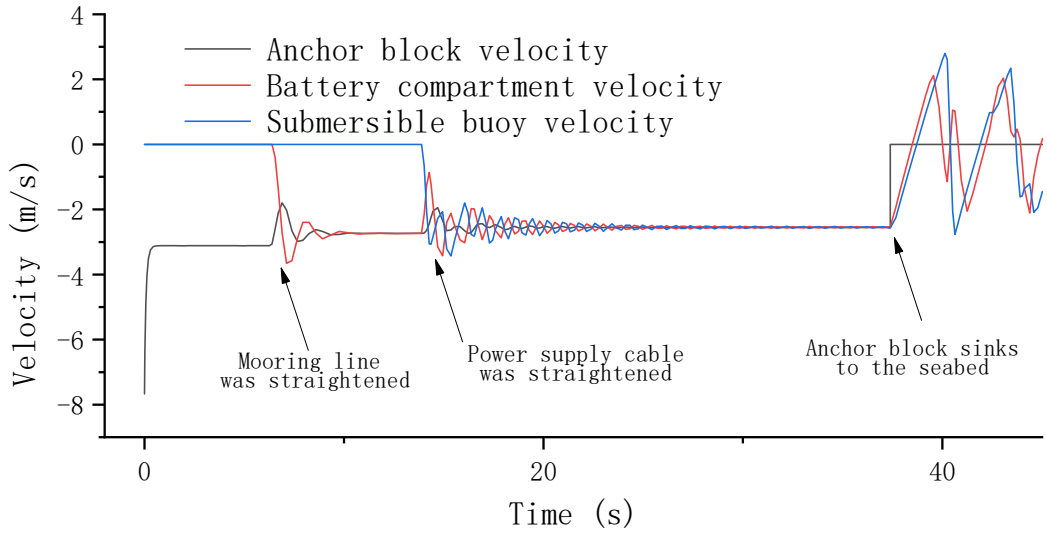


Figure 10. Velocity variation under 150 kg underwater net weight of anchor block.

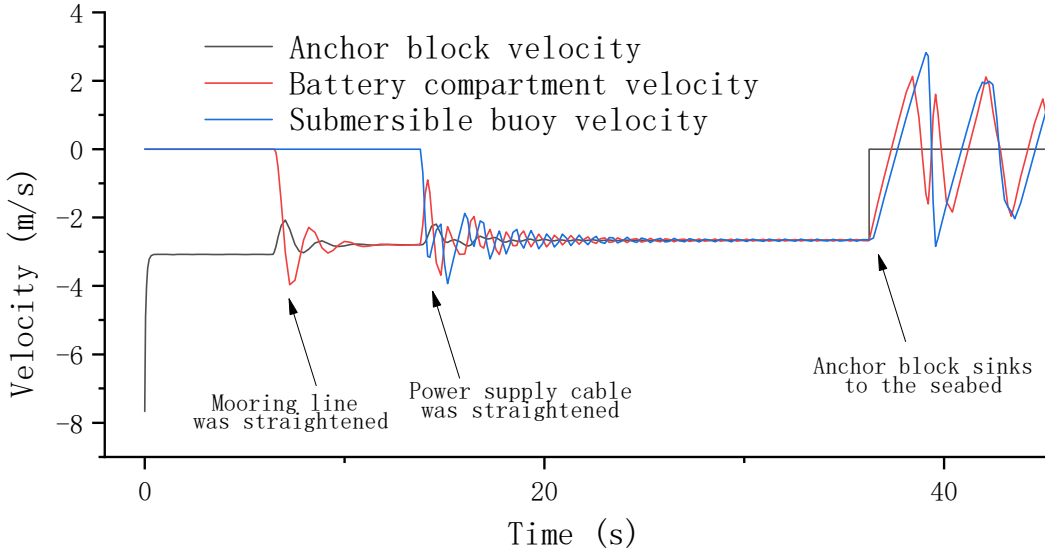


Figure 11. Velocity variation under 200 kg underwater net weight of anchor block.

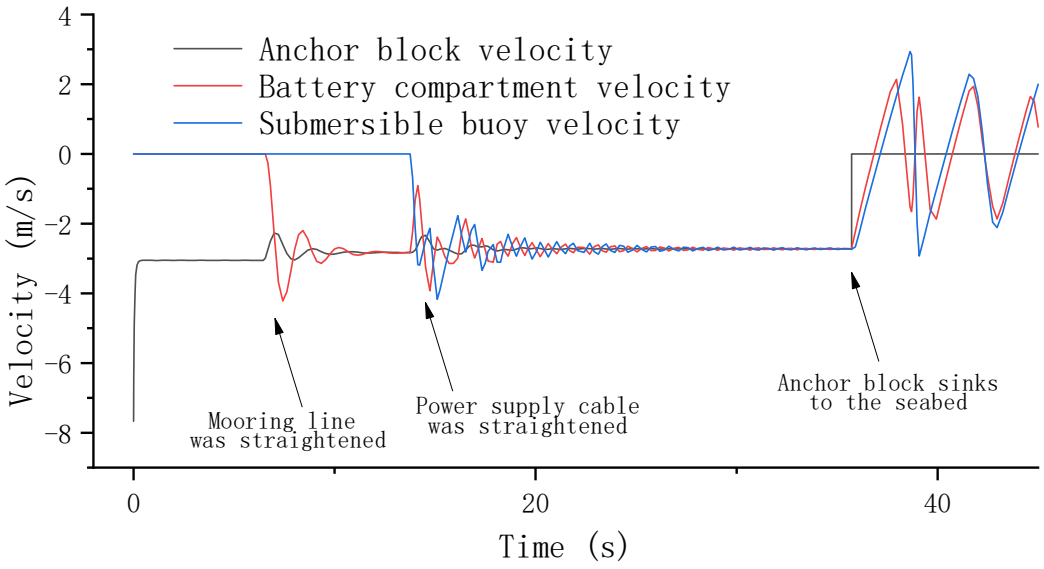


Figure 12. Velocity variation under 250 kg underwater net weight of anchor block.

By comparing submersible buoys under different anchor block weights, it can be seen that the velocity variation in marine submersible buoys has a similar velocity variation pattern. A submersible buoy system with a higher anchor block weight has a faster velocity in the deployment process and reaches the seabed sooner.

4.3. Tension Variation of Cables in Marine Submersible Buoy

The tension variations in the mooring line and power supply cable are illustrated in Figures 13–15. A large tension occurs when the mooring line and power supply cable are straightened by the anchor block. Then, the tension oscillates to a stable value. The greater the weight of the anchor block, the greater the tension. After the anchor block sinks to the seabed, the positive buoyancy of the battery compartment and buoy causes a large tension on the mooring line and power supply cable. The large tension after the anchor block sinks to the seabed is not relevant to the anchor block weight.

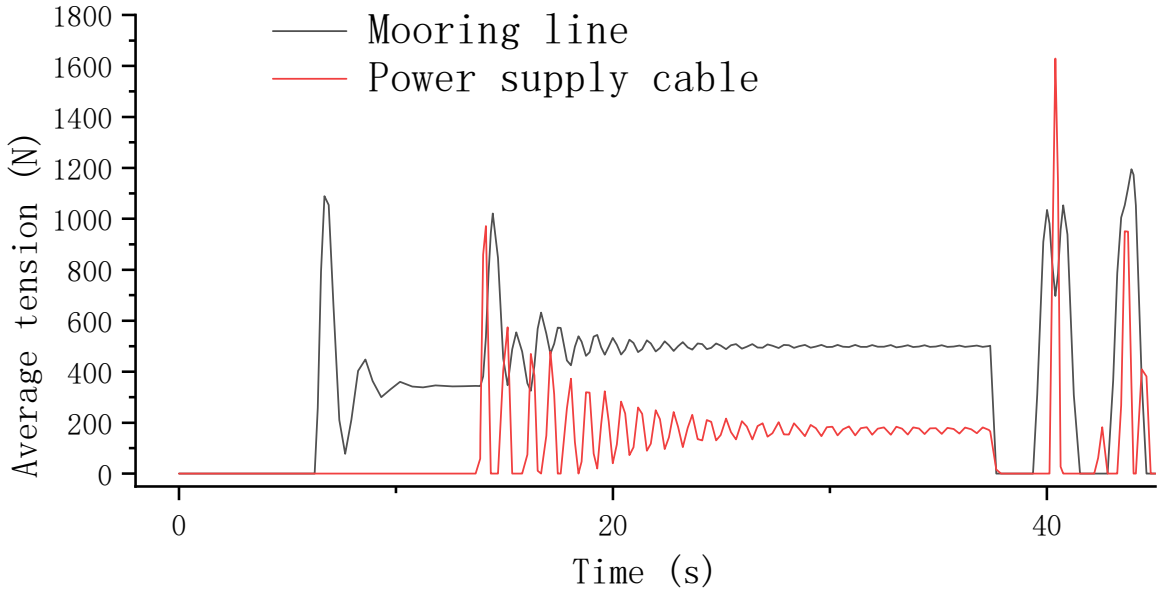


Figure 13. Tension variation under 150 kg underwater net weight of anchor block.

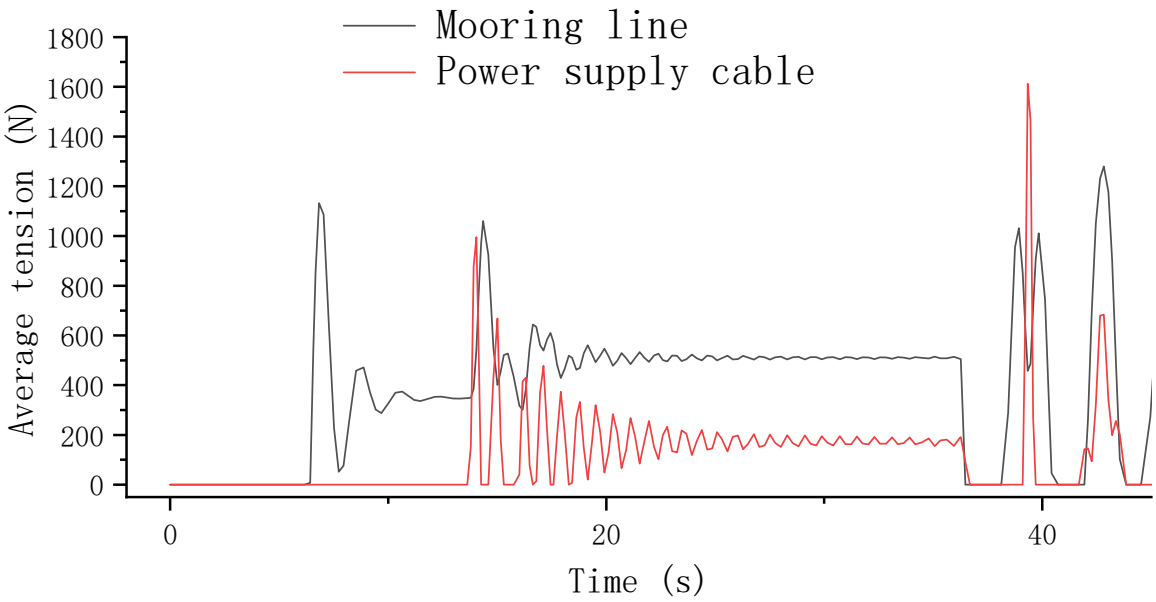


Figure 14. Tension variation under 200 kg underwater net weight of anchor block.

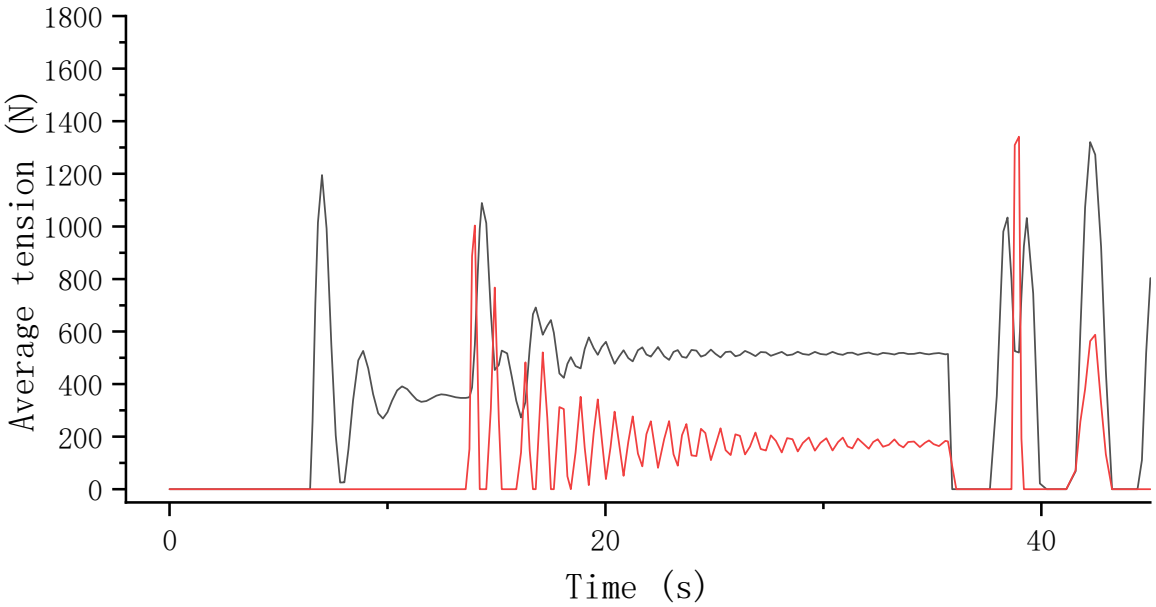


Figure 15. Tension variation under 250 kg underwater net weight of anchor block.

5. Optimization of Marine Submersible Buoy System

5.1. Particle Swarm Optimization

Particle swarm optimization is widely used in engineering optimization problems because it has a strong global search capability for nonlinear and multimodal problems. There have been plenty of successful examples of its use. Combined with penalty function, it can be applied to multi-objective optimization problems. Therefore, it is chosen to optimize the key parameters of a marine submersible buoy system.

The basic idea of particle swarm optimization is that, assuming a D-dimensional search space, a swarm consists of N particles, where the position of the particle indexed by i is represented by a D-dimensional vector, denoted as:

$$X_i = (x_{i1}, x_{i2}, \cdots, x_{iD}),\ i = 1, 2, \cdots, N \tag{11}$$

The flight velocity of each particle is a D-dimensional vector, denoted as:

$$V_i = (v_{i1},\ v_{i2}, \cdots, v_{iD}), i = 1, 2, \cdots, N \tag{12}$$

The individual best position found by the particle indexed by i up to the present moment is called the individual best, denoted as:

$$p_{\text{best}} = (p_{i1}, p_{i2}, \cdots, p_{iD}),\ i = 1, 2, \cdots, N \tag{13}$$

The global best position found by the particle swarm up to the present moment is referred to as the global best, denoted as:

$$g_{\text{best}} = (g_1, g_2, \cdots, g_D) \tag{14}$$

When these two best positions are found, each particle updates its velocity and position according to the following Equations (15) and (16):

$$v_{ij}(s+1) = v_{ij}(s) + c_1 r_1(s)\left[p_{ij}(s) - x_{ij}(s)\right] + c_2 r_2(s)\left[p_{gj}(s) - x_{ij}(s)\right] \tag{15}$$

$$x_{ij}(s+1) = x_{ij}(s) + v_{ij}(s+1) \tag{16}$$

where c_1 and c_2 are the learning factors; r_1 and r_2 are uniform random numbers in the range [0, 1]; s is the number of iterations; and v_{ij} represents the velocity of the particle. Randomness is added to the particle flight by r_1 and r_2. Three components make up the right-hand side of the equation: the momentum component, which reflects the particle's tendency to maintain its previous velocity; the cognitive component, which reflects the particle's tendency to approach its own historical best position; and the social component, which reflects the particle's tendency to approach the historical best positions of the swarm.

5.2. Optimization Model

In order to obtain an appropriate anchor block weight, mooring line length, and power supply cable length, particle swam optimization is applied to determine these key parameters. The case is that a submersible buoy system is deployed in a sea area with a 500 m depth. The position vector of the particle is in three dimensions. The first component of the position vector corresponds to the length of the mooring line. The second and third components correspond to the length of the power supply cable and the net underwater weight of the anchor block, respectively.

The weight of the anchor block should be greater than the sum weight of the battery compartment and submersible buoy, otherwise the anchor block cannot pull the battery compartment and submersible buoy into the water. The total length of the mooring line and power supply cable should not be too far away from a certain water level, otherwise the efficiency of the marine submersible buoy will decrease. Accordingly, the upper bound and lower bound are set to $\begin{bmatrix}30 & 30 & 300\end{bmatrix}$ and $\begin{bmatrix}10 & 10 & 90\end{bmatrix}$ respectively.

The penalty function method is used to constrain the particle position. The penalty function adds an obstacle function to the fitness function to constrain the position of the particles when solving the optimization problems. As illustrated in Figure 16, for particles with a rope length and tension exceeding a given value, the obstacle function is added. Their fitness is the landing time plus 2000. For particles with a rope length and tension not exceeding a given value, their fitness is the landing time.

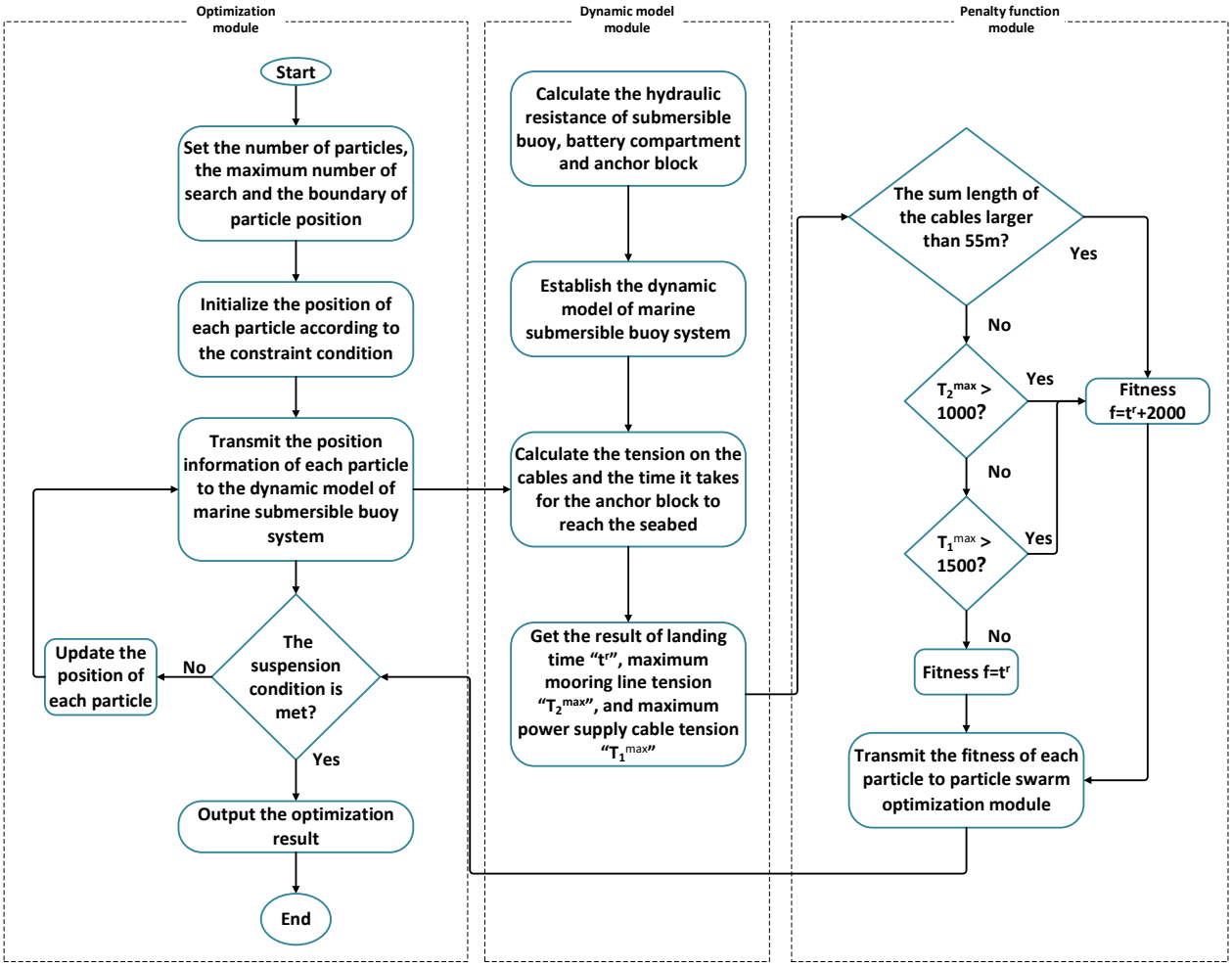


Figure 16. The running process of the optimization model.

5.3. Optimization Result and Discussion

The number of particles is set to 100. As illustrated in Figure 17, the fitness decreases rapidly in the initial iterations. After 50 iterations, the fitness is basically maintained at the same value. The final result of the particle position is $[24.83 \quad 29.78 \quad 228.81]$, which corresponds to a 24.83 m length of the mooring line, 29.78 m length of the power supply cable, and 228.81 kg anchor block underwater net weight.

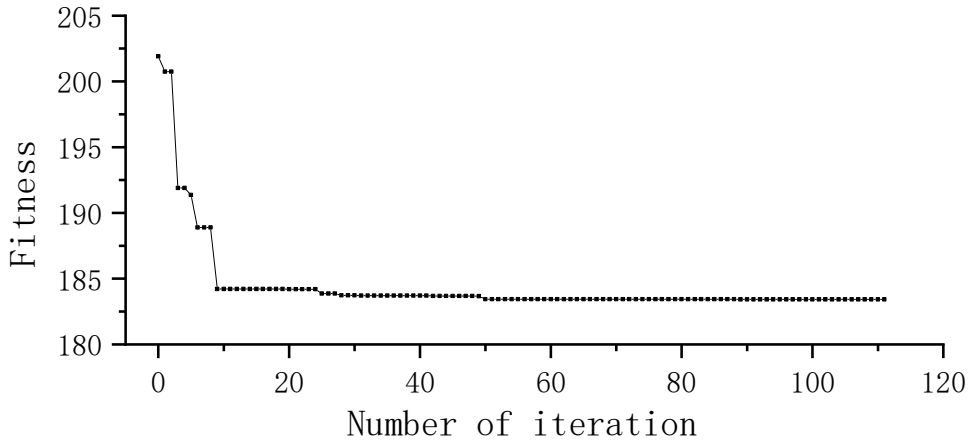


Figure 17. Variation in fitness value.

The final fitness value of the optimized result is 183.43, which means that the anchor block reaches the seabed 183.43 s after it is dropped into the water. Figures 18 and 19 illustrate the tension variation in the mooring line and power supply cable. It can be seen from these results that the tension of the mooring line and the power supply cable does not exceed the given value.

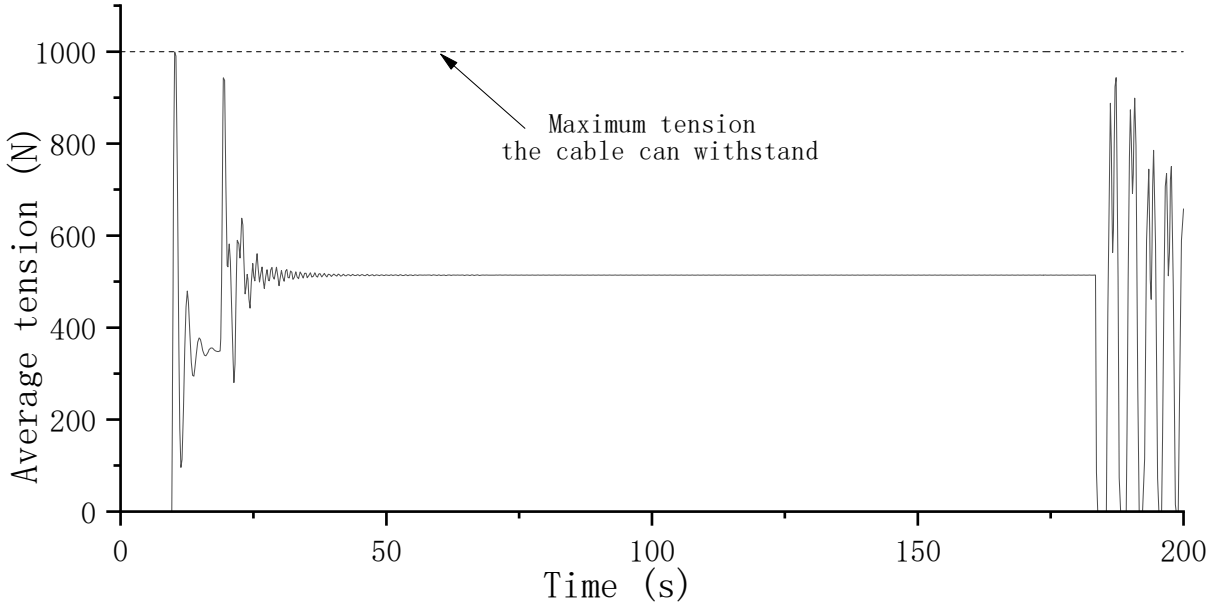


Figure 18. Mooring line tension variation.

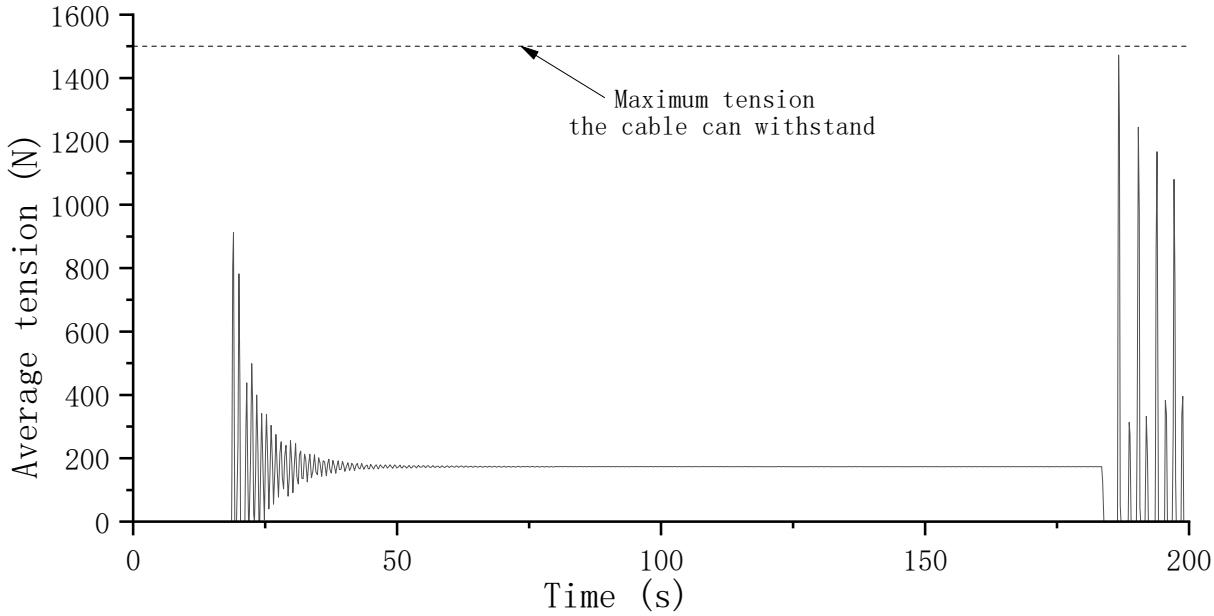


Figure 19. Power supply cable tension variation.

6. Conclusions

In this paper, the dynamic model of a marine submersible system is established based on computational fluid dynamics and multi-body dynamics. The dynamic equations are established and solved using the Runge–Kutta method of the fourth order. The dynamic mechanical behavior of the cables and the velocity variation of each component in the anchor-last deployment process are obtained. The results show that the velocity variations in marine submersible buoy systems under different anchor block weights have a similar

velocity variation pattern. A large tension occurs when the mooring line and power supply cable are straightened by the anchor block. After the anchor block sinks to the seabed, the cables are straightened because of the submersible buoy and battery compartment's positive buoyancy. This process causes a large tension on the cables.

In order to obtain the appropriate parameters, particle swarm optimization is used to optimize the key parameters. The penalty function is used to constrain the position of the particles. The results show that particle swarm optimization is effective in optimizing the marine submersible buoy system. The optimized result has a fast velocity in reaching the seabed and the tension on the cables does not exceed the maximum value. Therefore, the modeling and optimization methods proposed in this paper have reference value for the design and optimization of marine submersible buoy systems.

Author Contributions: Conceptualization, X.C., G.L. and B.L.; methodology, G.L. and B.L.; software, X.C. and G.L.; validation, B.L.; formal analysis, G.L.; investigation, X.C.; resources, B.L.; data curation, X.C. and G.L.; writing—original draft preparation, X.C. and B.L.; writing—review and editing, X.C. and B.L.; visualization, X.C., G.L. and B.L.; supervision, X.C. and G.L.; project administration, B.L. and G.L.; funding acquisition, X.C. and G.L. All authors have read and agreed to the published version of the manuscript.

Funding: This research received no external funding.

Institutional Review Board Statement: Not applicable.

Informed Consent Statement: Not applicable.

Data Availability Statement: Not applicable.

Conflicts of Interest: The authors declare no conflict of interest.

References

1. Da, L.; Wang, C.; Lu, X.; Han, M.; Deng, X. The characteristic analysis of ambient sea noise spectrum based on submersible buoy. *Acta Oceanol. Sin.* **2014**, *36*, 54–60.
2. Feng, S.; Wang, L.; Dong, L.; Li, Q. Design of data-sampling and high-capacity storage system in acoustic submersible buoy application. *J. Appl. Acoust.* **2014**, *33*, 81–86.
3. Xing, Y.; Wang, Z.; Liu, Z.; Xiang, X.; Yu, Y.; Xu, Y. Underwater Acoustics Data Acquisition System Based on Submersible Buoy. *Meas. Control Technol.* **2015**, *34*, 28–30,34.
4. Zhang, H.; Cao, W.; Wu, Z.; Song, X.; Wang, J.; Yan, T. Biofouling on deep-sea submersible buoy systems off Xisha and Dongsha Islands in the northern South China Sea. *Int. Biodeterior. Biodegrad.* **2015**, *104*, 92–96. [CrossRef]
5. Meng, K.; Qin, H.; Zhu, X.; Hou, F. Design and test of a new mobile submersible deep-sea seismic recording system. *J. Trop. Oceanogr.* **2020**, *39*, 49–56.
6. Kennedy, J.; Eberhart, R. Particle Swarm Optimization. In Proceedings of the Icnn95-International Conference on Neural Networks, Perth, WA, Australia, 27 November–1 December 1995.
7. Shul'ga, N.A.; Bezverkhii, A.I. Lagrangian description and numerical analysis of a discrete model of flexible systems. *Int. Appl. Mech.* **2004**, *40*, 1398–1404. [CrossRef]
8. Wang, J.; Luan, X. Shell failure and deformation of the submersible buoy under high pressure condition. *Mar. Sci. Bull.* **2010**, *29*, 481–487.
9. Lai, B.; Zhao, C.; Chen, X.; Tang, Y.; Lin, W. A Novel Structural Form of Semi-Submersible Platform for a Floating Offshore Wind Turbine with Hydrodynamic Performance Analysis. In *Applied Mechanics and Materials*; Trans Tech Publications Ltd.: Stafa-Zurich, Switzerland, 2014; pp. 109–113.
10. Qiao, D.; Yan, J.; Ou, J. Effects of Mooring Line with Buoys System on the Global Responses of a Semi-Submersible Platform. *Brodogradnja* **2014**, *65*, 79–96.
11. Qui, Z.; Jia, L.; Qin, Y.; Zhang, S.; Sun, X. Dynamic Modeling and Simulating Analysis of Submersible Buoy System. In *Applied Mechanics and Materials*; Trans Tech Publications Ltd.: Stafa-Zurich, Switzerland, 2014; pp. 1391–1396.
12. Tsukada, R.I.; Shiguemoto, D.A.; Morooka, C.K. Numerical Simulation of Vim Response of a Submersible Buoy Using a Semi-Empirical Approach. In Proceedings of the 33rd International Conference on Ocean, Offshore and Arctic Engineering, San Francisco, CA, USA, 8–13 June 2014; Volume 2.
13. Fontoura, D.V.R.; Tsukada, R.I.; Shiguemoto, D.A. Numerical Simulation of a Submersible Buoy Using a Wake Oscillator Model Calibrated for Vim. In Proceedings of the ASME 34th International Conference on Ocean, Offshore and Arctic Engineering, St. John's, NL, Canada, 31 May–5 June 2015; Volume 2.
14. Ji, C.; Yuan, Z. Experimental study of a hybrid mooring system. *J. Mar. Sci. Technol.* **2015**, *20*, 213–225. [CrossRef]

15. Zheng, Z.; Xu, J.; Huang, P.; Wang, L.; Yang, X.; Chang, Z. Dynamics of Anchor Last Deployment of Submersible Buoy System. *J. Ocean. Univ. China* **2016**, *15*, 69–77. [CrossRef]
16. Chen, J.; Hu, Z.; Duan, F. Comparisons of dynamical characteristics of a 5 MW floating wind turbine supported by a spar-buoy and a semi-submersible using model testing methods. *J. Renew. Sustain. Energy* **2018**, *10*, 053311. [CrossRef]
17. Ghafari, H.; Dardel, M. Parametric study of catenary mooring system on the dynamic response of the semi-submersible platform. *Ocean. Eng.* **2018**, *153*, 319–332. [CrossRef]
18. Yan, J.; Qiao, D.; Ou, J. Optimal design and hydrodynamic response analysis of deep water mooring system with submerged buoys. *Ships Offshore Struct.* **2018**, *13*, 476–487. [CrossRef]
19. Yang, Q.; Zheng, Y.; Wang, Z.; Zhang, Y.; Hao, Z. The Influence of Vertical Cable on Flow Field and Acoustic Analysis of a Submersible Buoy System Based on CFD. In Proceedings of the 2019 14th IEEE Conference on Industrial Electronics and Applications (ICIEA), Xi'an, China, 19–21 June 2019; pp. 53–57.
20. Zhang, Y.; Zheng, Y.; Wang, Z.; Yang, Q.; Hao, Z. Flow Noise Assessment and Analysis of Submersible Buoy Based on FEM/AML Method. In Proceedings of the 2019 14th IEEE Conference on Industrial Electronics and Applications (ICIEA), Xi'an, China, 19–21 June 2019; pp. 1386–1391.
21. Zhilei, Z.; Peng, M.; Houbing, L.; Kun, H.; Feng, L.; Ge, J. A Low-Power DAQ System with High-Speed Storage for Submersible Buoy. In Proceedings of the 2019 IEEE 2nd International Conference on Electronics Technology (ICET), Chengdu, China, 10–13 May 2019; pp. 400–403.
22. Touzon, I.; Nava, V.; Gao, Z.; Mendikoa, I.; Petuya, V. Small scale experimental validation of a numerical model of the HarshLab2.0 floating platform coupled with a non-linear lumped mass catenary mooring system. *Ocean. Eng.* **2020**, *200*, 107036. [CrossRef]
23. Chandrasekaran, S.; Uddin, S.A.; Wahab, M. Dynamic Analysis of Semi-submersible Under the Postulated Failure of Restraining System with Buoy. *Int. J. Steel Struct.* **2021**, *21*, 118–131. [CrossRef]
24. Rong, X.; Dou, P.; Chen, J. Time-domain coupling analysis of semi-submersible floating foundation with four buoys for offshore wind turbine and its mooring system. *J. Phys. Conf. Ser.* **2021**, *2005*, 012208. [CrossRef]
25. Amaechi, C.V.; Wang, F.; Ye, J. Experimental Study on Motion Characterisation of CALM Buoy Hose System under Water Waves. *J. Mar. Sci. Eng.* **2022**, *10*, 204. [CrossRef]
26. Amaechi, C.V.; Wang, F.; Ye, J. Numerical studies on CALM buoy motion responses and the effect of buoy geometry cum skirt dimensions with its hydrodynamic waves-current interactions. *Ocean. Eng.* **2022**, *244*, 110378. [CrossRef]
27. Chen, X.; Liu, B.; Le, G. Numerical Simulation Research on the Anchor Last Deployment of Marine Submersible Buoy System Based on VOF Method. *J. Mar. Sci. Eng.* **2022**, *10*, 1681. [CrossRef]
28. Han, D.; Wang, W.; Li, X.; Su, X. Optimization design of multiple tuned mass dampers for semi-submersible floating wind turbine. *Ocean. Eng.* **2022**, *264*, 112536. [CrossRef]
29. Li, M.; Liu, Y.; Liu, Y.; Chen, G.; Tang, Q.; Han, Y.; Wen, Y. Simulative Evaluation of the Underwater Geodetic Network Configuration on Kinematic Positioning Performance. *Remote Sens.* **2022**, *14*, 1939. [CrossRef]
30. Neisi, A.; Ghassemi, H.; Iranmanesh, M.; He, G. Effect of the multi-segment mooring system by buoy and clump weights on the dynamic motions of the floating platform. *Ocean. Eng.* **2022**, *260*, 111990. [CrossRef]
31. Harlow, F.H.; Nakayama, P.I. Turbulence Transport Equations. *Phys. Fluids* **1967**, *10*, 2323–2332. [CrossRef]
32. Gao, T.; Wang, Y.; Pang, Y.; Cao, J. Hull shape optimization for autonomous underwater vehicles using CFD. *Eng. Appl. Comput. Fluid Mech.* **2016**, *10*, 601–609. [CrossRef]

Disclaimer/Publisher's Note: The statements, opinions and data contained in all publications are solely those of the individual author(s) and contributor(s) and not of MDPI and/or the editor(s). MDPI and/or the editor(s) disclaim responsibility for any injury to people or property resulting from any ideas, methods, instructions or products referred to in the content.